

# Scintillation Counters for the DØ Muon Upgrade

B.S. Acharya<sup>o</sup>, B. Baldin<sup>f</sup>, S. Banerjee<sup>o</sup>, S.B. Beri<sup>m</sup>,  
 V. Bhatnagar<sup>m</sup>, M. Bhattacharjee<sup>e</sup>, A. Brandt<sup>f</sup>, R. Brock<sup>j</sup>,  
 J.M. Butler<sup>b</sup>, S. Chopra<sup>m</sup>, M. Cummings<sup>g</sup>, D. Denisov<sup>f</sup>,  
 H.T. Diehl<sup>f</sup>, S.R. Dugad<sup>o</sup>, P. Duggan<sup>j</sup>, S. Fahey<sup>j</sup>, E. Flattum<sup>f</sup>,  
 M. Fortner<sup>l</sup>, V. Glebov<sup>n</sup>, J. L. González Solís<sup>d</sup>, D.R. Green<sup>f</sup>,  
 J. Green<sup>l</sup>, N. Grossman<sup>f</sup>, A. Gupta<sup>o</sup>, H. Haggerty<sup>f</sup>,  
 S. Hansen<sup>f</sup>, R. Hatcher<sup>j</sup>, D. Hedin<sup>l</sup>, R. Hernández-Montoya<sup>d</sup>,  
 T. Hu<sup>f</sup>, S. Igarashi<sup>f</sup>, A.S. Ito<sup>f</sup>, S.A. Jerger<sup>j</sup>, K. Johns<sup>a</sup>,  
 S.D. Kalmani<sup>o</sup>, J.M. Kohli<sup>m</sup>, M.R. Krishnaswamy<sup>o</sup>,  
 R. Markeloff<sup>l</sup>, T. Marshall<sup>h</sup>, T. McMahon<sup>i</sup>, D. Miller<sup>f</sup>,  
 N.K. Mondal<sup>o</sup>, P. Nagaraj<sup>o</sup>, V.S. Narasimham<sup>o</sup>,  
 A. Narayanan<sup>a</sup>, M. Nicola<sup>c</sup>, M. Nila<sup>j</sup>, N. Parua<sup>o</sup>, B.G. Pope<sup>j</sup>,  
 P.Z. Quintas<sup>f</sup>, M.V.S. Rao<sup>o</sup>, L.V. Reddy<sup>o</sup>, T. Regan<sup>f</sup>,  
 T. Rockwell<sup>j</sup>, B. Satyanarayana<sup>o</sup>, H.C. Shankar<sup>o</sup>, J.B. Singh<sup>m</sup>,  
 P.M. Sood<sup>m</sup>, A. Taketani<sup>f</sup>, P.R. Vishwanath<sup>o</sup>, J. Wilcox<sup>k</sup>,  
 D.R. Wood<sup>k</sup>, R. Yamada<sup>f</sup>, T. Yasuda<sup>k</sup>

<sup>a</sup>*University of Arizona, Tucson, Arizona 85721, USA*

<sup>b</sup>*Boston University, Boston, Massachusetts 02215, USA*

<sup>c</sup>*LAFEX, Centro Brasileiro de Pesquisas Físicas, Rio de Janeiro, Brazil*

<sup>d</sup>*CINVESTAV, Mexico City, Mexico*

<sup>e</sup>*Delhi University, Delhi, India 110007*

<sup>f</sup>*Fermi National Accelerator Laboratory, Batavia, Illinois 60510, USA*

<sup>g</sup>*University of Hawaii, Honolulu, Hawaii 96822, USA*

<sup>h</sup>*Indiana University, Bloomington, Indiana 47405, USA*

<sup>i</sup>*Langston University, Langston, Oklahoma 73050, USA*

<sup>j</sup>*Michigan State University, East Lansing, Michigan 48824, USA*

<sup>k</sup>*Northeastern University, Boston, Massachusetts 02115, USA*

<sup>l</sup>*Northern Illinois University, DeKalb, Illinois 60115, USA*

<sup>m</sup>*University of Panjab, Chandigarh 16-00-14, India*

<sup>n</sup>*University of Rochester, Rochester, New York 14627, USA*

<sup>o</sup>*Tata Institute of Fundamental Research, Colaba, Mumbai 400005, India*

(for the DØ Collaboration)

---

**Abstract**

We present the results of an upgrade to the DØ muon system. Scintillating counters have been added to the existing central DØ muon system to provide rejection for cosmic ray muons and out-of-time background, and to provide additional fast timing information for muons in an upgraded Tevatron. Performance and results from the 1994–1996 Tevatron run are presented.

---

Submitted to Nuclear Instruments and Methods in Physics Research,  
Section A

## 1 Introduction

The DØ detector at the Fermilab Tevatron was completed in 1992 and took data during the 1992-1993 Tevatron Collider run (Run 1a) and from 1994-1996 (Run 1b and 1c). This paper describes a scintillator upgrade to the DØ wide angle muon system which was fabricated for Run 1b and 1c. A cutaway isometric view of the detector is shown in Fig. 1 where the central detectors, calorimeter, and muon detectors are shown.

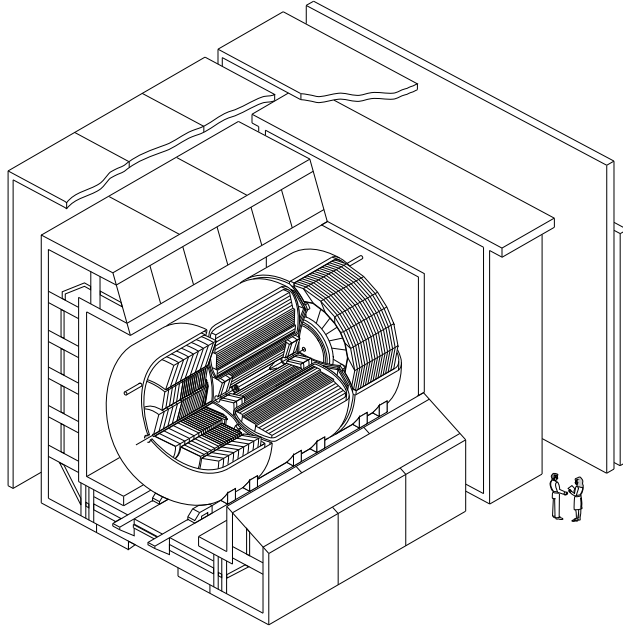


Fig. 1. An isometric view of the DØ detector.

The DØ wide angle muon system consists of three separate solid iron toroid magnets with three sets of proportional drift tube chambers (PDT's) to measure track coordinates for each muon. The first set of chambers (A layer) are located between the beamline and the toroid and provide a closely spaced set of measurements of the muon track and determine the entrance point into the toroid. The second (B layer) and third (C layer) set of chambers, located after the toroid, are separated by 1 m and yield the exit direction. The bend in the toroid is in a plane which approximately goes through the center of the Tevatron beam pipe.

Due to the large PDT drift space the drift times extend to as much as  $0.9 \mu\text{sec}$ . The accelerator operated with 6 bunches in the collider for Run 1 which gave a  $3.5 \mu\text{sec}$  time gap between collisions. The next collider run (Run 2) is scheduled to operate with 36 or more bunches which will have a crossing time of  $0.396$  or  $0.132 \mu\text{sec}$ . In order to label the muon in the PDT with the appropriate

bunch crossing, a fast timing reference will be required. Furthermore, the long livetime coupled with an increased instantaneous luminosity would increase the cosmic ray coincidence rate to an unacceptable level. The solution to this problem, for the central region, was to add scintillation counters to the outside of the muon system. The counters were installed in Run 1b as part of the upgrade for Run 2. The counters provided cosmic ray rejection. In addition the counters provided rejection of backscattered particles which were found to have a significant effect on the trigger.

The scintillation counters were installed on the sides and top of the central muon system (CF). The scintillation counters spanned a region of  $|\eta| \leq 1$  and covered 6 of the 8 octants in azimuth where each octant consisted of 40 scintillation counters. The octants were numbered from 0 to 7 in increasing azimuth, such that octants 1 and 2 covered the top quadrant of the detector. Counters were not installed on the bottom or ends ( $|\eta| \geq 1$ ) of the DØ detector. Bottom counters, which could not be installed while the detector was in the collision hall, will be added before Run 2. End counters required a different design due to the high multiplicities in this region. End counters will also be added for Run 2. Prototype end counters were tested during Run 1b and 1c. This document describes only the Run 1 counters.

Figure 2 is an elevation view of the detector, which shows the detector systems mentioned above and the location of the top scintillation counters. Also shown is the Tevatron beam pipe centered within the detector. The muon system has been described in previous publications [1] and so will not be discussed in any more detail here.

## 2 Scintillation Counter Design

The 240 scintillation counters cover the outside layer of PDTs in the central region. There are three different lengths of scintillation counters to match the three different sizes of the PDT's, with the long dimension of the scintillation counter chosen to match the long dimension of the PDT cell (see Table 1). There are 8 counters per PDT module in two overlapping layers as shown in Fig. 3. The corners on one end of the scintillator are cut at a  $45^\circ$  angle to allow counters to be nested. The final configuration of two layers provided approximately 1 to 2 cm overlap to minimize the dead area (see Fig. 3). Figure 4 shows a close up view of the top of a scintillation counter.

The scintillation counters were fabricated at Fermilab and the Tata Institute of Fundamental Research (TIFR) in India using Bicron 404A scintillator [2]. The Bicron 404A scintillator was chosen because of its low cost and good performance. It was approximately a factor of two less expensive than compa-

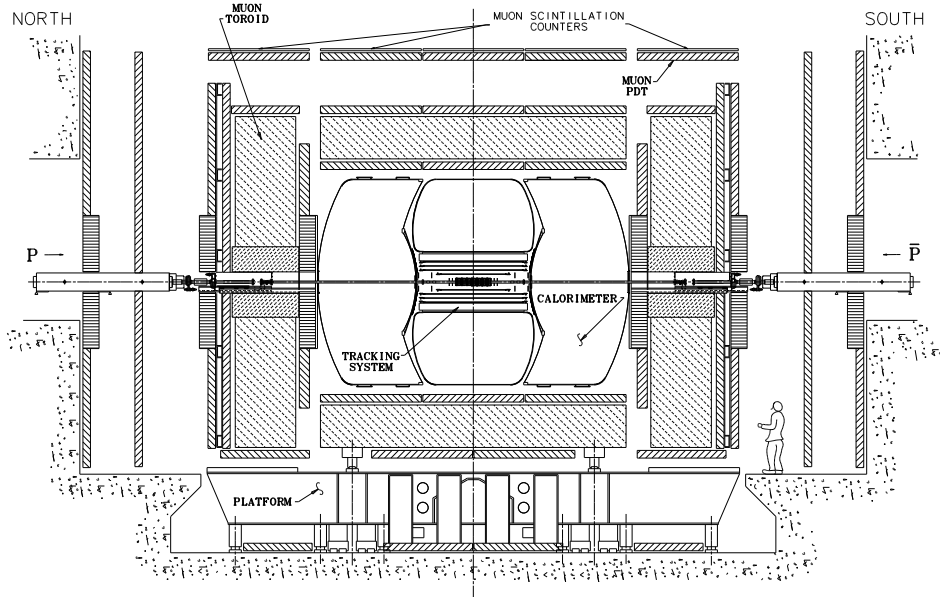


Fig. 2. An elevation view of the DØ detector showing the location of the muon scintillation counters.

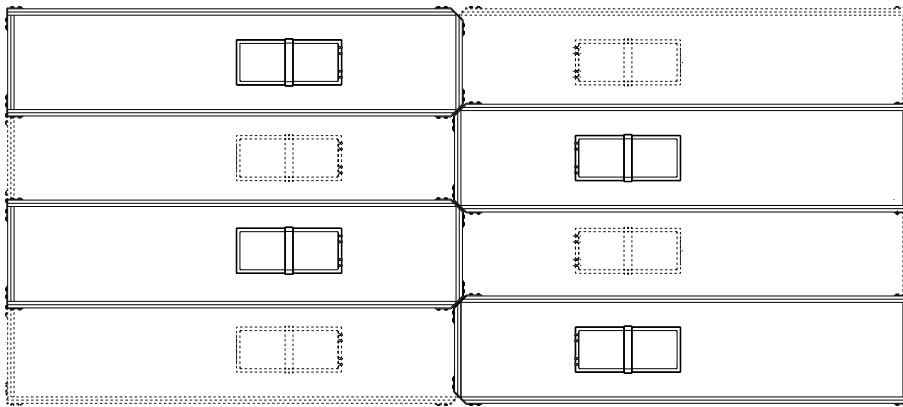


Fig. 3. The nested configuration of eight scintillation counters for a muon PDT module. The counters represented by the solid lines are offset in height relative to the counters drawn with the dotted lines.

rable scintillators. The relatively short attenuation length of this scintillator was not a problem because the light was collected within a short distance by wavelength shifting fibers. The scintillator was machined with 4 mm wide straight grooves 1.75 mm deep on one side (see Fig. 5). The grooves on each half of the scintillator were offset so that they would not overlap in the center. The half of the scintillator with the 45° corners had one more groove than the other half. The machining was done using computer controlled milling heads at Lab 8 at Fermilab, a commercial company in Rockford IL [3], and

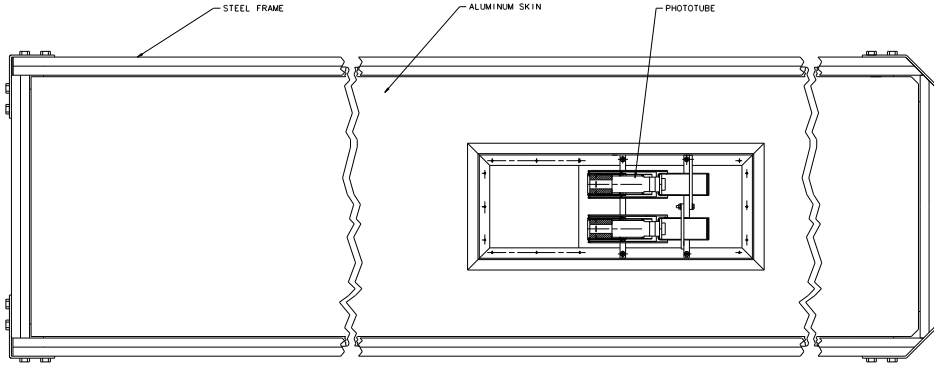


Fig. 4. The top view of a muon scintillation counter showing the support frame and the location of the photomultiplier tubes and cover.

Length (in)	Width (in)	Depth (in)	grooves	fibers/pmt
81.5	25.0	0.5	78/79	314
108.0	25.0	0.5	78/79	314
113.0	25.0	0.5	78/79	314

Table 1

The three sizes of muon scintillation counters.

at the central workshop of Bhabha Atomic Research Center, Bombay [4]. The grooves were machined with 8 mm spacing and covered roughly half the area of one face of the scintillator. Four 1 mm diameter Bicron BCF91A wavelength shifting fibers [5] were placed in each groove. The fibers were brought

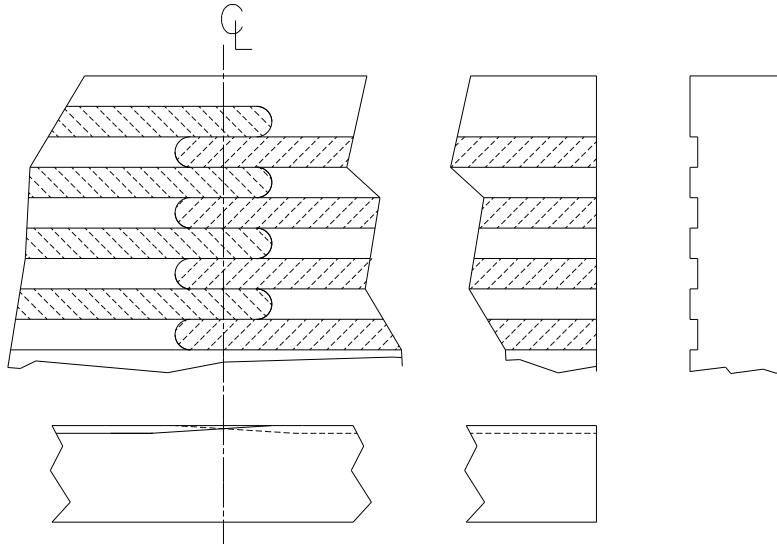


Fig. 5. The top, side, and end views of the grooves in the scintillator are shown. In each groove are epoxied four waveshifting fibers.

to the center of the counter to be viewed by phototubes. Each fiber covers half the length of the counter. This center readout geometry was chosen to reduce the attenuation of the light in the fiber and also reduce the time jitter due to light transmission in the fiber. For the 81.5" counters built at TIFR, the edge grooves were loaded with Kuraray Y-11 [6] double clad fibers to increase the light output at the edge of the counters. The double clad fibers provide a factor of 1.8 more light than a single clad fiber due to a more efficient capture of the wavelength shifted light and also due to a longer attenuation length in the fiber. The double clad fibers were only used on the edges since they were about five times more expensive than single clad fiber.

The fibers were held in place with Bicon 600 optical epoxy [7] at seven locations along the groove. Five minute epoxy [8] was used at the ends of counters where the fibers extended beyond the scintillator. Both ends of the scintillator were diamond polished using a diamond cutter manufactured at Michigan State University (MSU) [9] and brought to Fermilab and retrofitted for this project. For the counters made at TIFR, a custom made diamond polisher machine [10] was constructed. In order to increase the light yield a 1/32" anodized aluminum sheet [11] was placed on the diamond polished ends and held in place with aluminized mylar tape. The fibers going to the 45° cut corners were sputtered with aluminum at Fermilab's Lab 7 facility, and with an electron beam heating method at TIFR.

Two of the four fibers from each groove were epoxied into the hole of an acrylic cookie using five minute epoxy. The other two fibers from each groove were bundled and bonded to a second cookie. The fibers were rough cut with a saw and then the ends of cookies and the fibers were polished with the diamond cutter.

The counters were then wrapped with a Tyvek [12,13] sheet with a hole cut for the fibers and cookies. Tests comparing the Tyvek wrap to aluminum foil and aluminized mylar showed that the Tyvek improved the counter response by about 10%. A 3" wide black tape was used to secure the Tyvek sheet and cover any holes or seams. A 1/4" thick, closed cell polyethylene foam was placed on the top of the scintillator. The top and bottom surface of the scintillator were then covered with a 0.020" thick aluminum sheet (see Fig. 4). An 8" × 7 13/32" opening was cut in the top sheet for the fiber bundles and an aluminum angle lip was mounted around this hole. The aluminum sheets were taped together around the perimeter of the counter. In order to provide the support for the counter, commercially available steel channel frame [14] was placed over the aluminum sheets around the edges and bolted together. The counters then had metal bands attached at the center for additional support.

A plastic cover was used to provide access to the photomultiplier tubes. The plastic cover was fastened to the aluminum angle with velcro and the seams

were taped. SHV and BNC connectors for the high voltage and output signal were bolted to the cover for each phototube. Figure 6 shows an end view of a scintillation counter detailing the location of the photomultiplier tubes and cover.

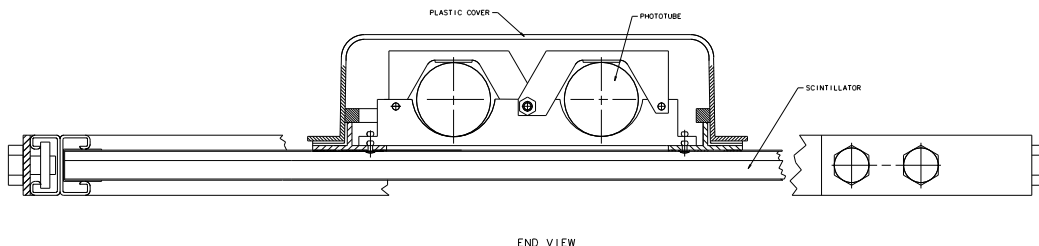


Fig. 6. The end view of a muon scintillation counter.

## 2.1 Fiber

The properties of the Bicon 91A waveshifting fiber were studied as part of the counter research and development work. The Bicon 91A waveshifting fiber was designed to be used in conjunction with the Bicon 404A scintillator. The light output from the fiber was tested with a variety of reflective surfaces at the far end of the fiber. The fibers were tested with the far end having a razor cut alone, diamond polished alone, diamond polished with aluminized mylar tape added, and diamond polished with the end sputtered with aluminum. The sputtered aluminum had the highest light output followed by the aluminized tape.

The measurements were made at the fiber testing facility at Fermilab [15]. The 1 mm diameter fibers were cut into 3 m lengths. Excitation was done at 30 cm intervals throughout the length of the fiber using ultraviolet light from a pencil source [16]. The light from the fiber was detected using a silicon photodiode [17] whose current was measured with a picoammeter. The entire system was operated under microcomputer control.

Each end of the fiber was epoxied into an acrylic ferrule and one end of the fiber was coated with optical grease [18] and clamped, using the ferrule, to the photodiode.

The measured intensity was fit by the sum of two exponentials of the form:

$$I(x) = A_1 \cdot \exp(-x/\alpha_1) + A_2 \cdot \exp(-x/\alpha_2) \quad (1)$$

where  $A_1$ ,  $A_2$ ,  $\alpha_1$ , and  $\alpha_2$  are the fitted parameters and  $x$  is the position along the fiber. Figure 7 shows the fit to the relative intensity for an arbitrary fiber.

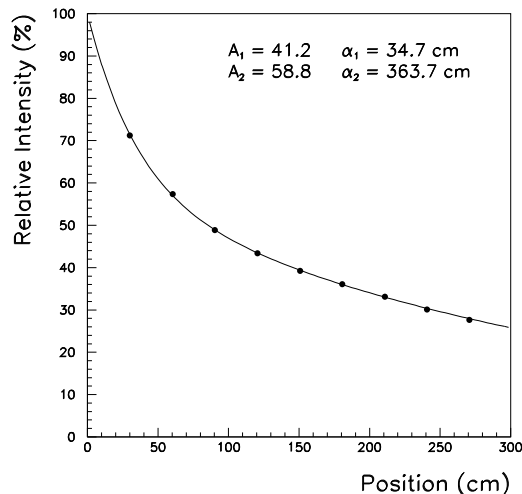


Fig. 7. The relative intensity as a function of the excitation location along the fiber.

The long attenuation term is due to the light in the core of the fiber and the short attenuation length term is due to the light transmitted in the cladding of the fiber.

The maximum light output was observed for diamond polished and sputtered fibers which yielded 65% more light output than the razor cut fibers. The light output with diamond polished fibers and aluminized mylar tape was about 10% less than the aluminum sputtered fiber.

The above studies led us initially to use the diamond polished fibers with an aluminized mylar tape over the sputtered fibers, because the time required to sputter the 150,000 fibers exceeded the time limit for construction of the system. However, for the final design, an anodized aluminum strip [11] was placed over the ends since the aluminized tape formed bubbles in the adhesive. The light output from this design was shown to be stable over time.

## 2.2 Phototube

The 1.5" diameter EMI 9902KA photomultiplier tube [19] was selected for readout of the light produced by the scintillator. A number of criteria determined the selection of this phototube. Space limitations dictated the diameter, the phototube had to match the light emission characteristics of the waveshifter fiber, thus the photocathode required a spectral response which

extended into the green region. Also required were an amplification of  $10^7$  and a dark current of less than 10 nA. The tubes were required to be fast and have a rise time of less than 3 nsec.

Since fibers from different parts of the counter were randomly positioned on the photocathode face, we investigated the response of the EMI 9902KA as a function of position on the photocathode at Fermilab's phototube testing facility. Light from an ultraviolet laser was brought via an optical fiber to illuminate  $\sim 2$  mm spot on the PMT photocathode. The response, in arbitrary units, as a function of position is shown in Fig. 8 for a typical 9902KA phototube. The fibers from our counters formed a bundle  $7/8$ " in diameter at the photocathode and so were well matched to the high response region of the PMT.

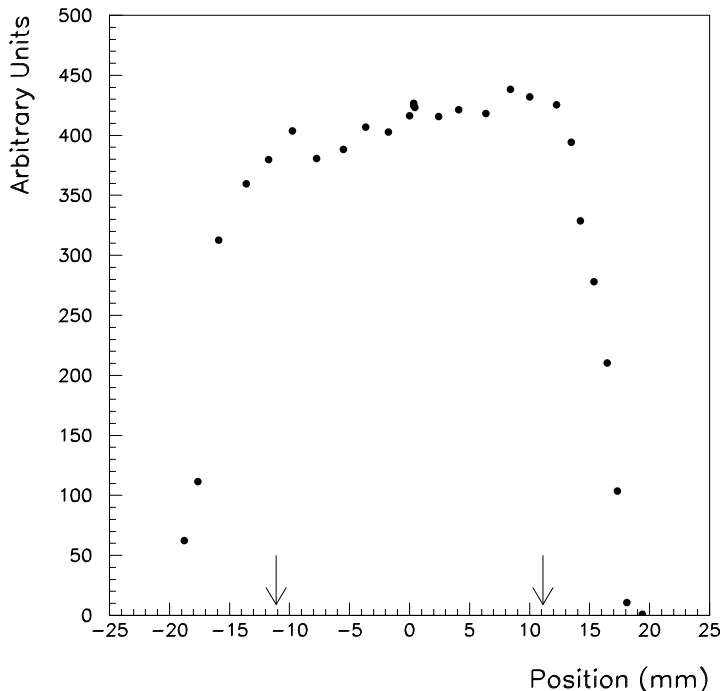


Fig. 8. Relative response across the face of the photocathode for an EMI 9902KA phototube where zero is the center of the photocathode. The arrows delineate the region where the fiber is incident upon the photocathode.

For compatibility with the DØ High Voltage system, the photomultiplier base voltage divider and readout circuit (see Fig. 9) was required to draw a low current: 0.2 mA at a cathode-anode voltage of +2 kV. The resistor values chosen to meet this requirement were 2.5:1.2:1.2:1.0 for the first, second, third, and remaining stages. To minimize output noise into the scintillator electronics readout cards the output signal was filtered to reduce low frequency(ac) noise and the signal ground isolated from the common (HV) ground. The input

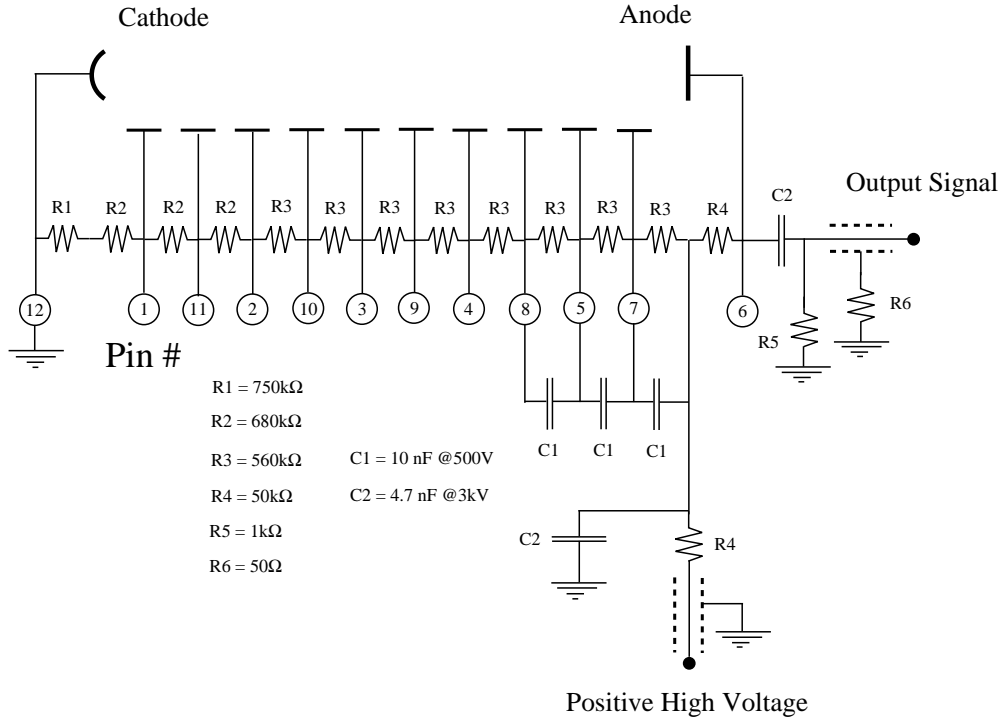


Fig. 9. The circuit diagram for the photomultiplier base.

HV was also filtered and capacitors were used across the last three stages to prevent voltage sagging.

Due to tight space constraints in several areas of the detector where counters were to be installed, the base assembly was required to be compact. The base circuit was mounted on a  $1.75'' \times 1.5''$  printed circuit board (PCB), connected by a standoff to a circular PCB  $1.5''$  in diameter which was fitted onto a Hamamatsu socket [20]. This assembly was conformally coated and fitted inside a  $2'' \times 4''$  cylindrical aluminum container, which provided electromagnetic shielding, with the socket protruding through one end. Readout and HV connections were made through an isolated BNC and an SHV bulkhead mounted on a  $2''$  diameter aluminum cap which was secured onto the end of the cylinder. To insure the consistency of the large number (800) of bases produced, the PCBs were manufactured [21], stuffed, and assembled by outside vendors [22].

The phototube and base were secured to the cookie using a spring mechanism which attached to the cookie and to the aluminum cap. This ensured the photocathode was centered on the cookie and flush with the surface. Surrounding this assembly was placed a Model 17P37 magnetic shield [23] to protect the phototube from magnetic fields. In addition, the entire assembly was surrounded by a second  $1/8''$  thick, iron shield to ensure good magnetic field protection.

### 3 Scintillation Counter Electronics

The block diagram for the scintillation counter trigger board (SCTB) is shown in Fig. 10. There was one electronics board for each group of 8 scintillation counters (16 phototubes) which were mounted on a muon system PDT. Each board had 16 signal processing channels, trigger logic, a test pulse generator, timing controls and a 1553B bus interface for control and status. Each scintillator channel could be remotely enabled or disabled using an enable bit register. The 1553 bus is the standard used by the DØ experiment for downloading and monitoring the front end electronics. The timing control circuit was a programmable gate generator linked to the transition of a muon system timing signal. The trigger logic generated output trigger signals based on the inputs and the AND/OR settings for each channel. The test pulse generator simulated the scintillation counters signal and could be synchronized to different sources.

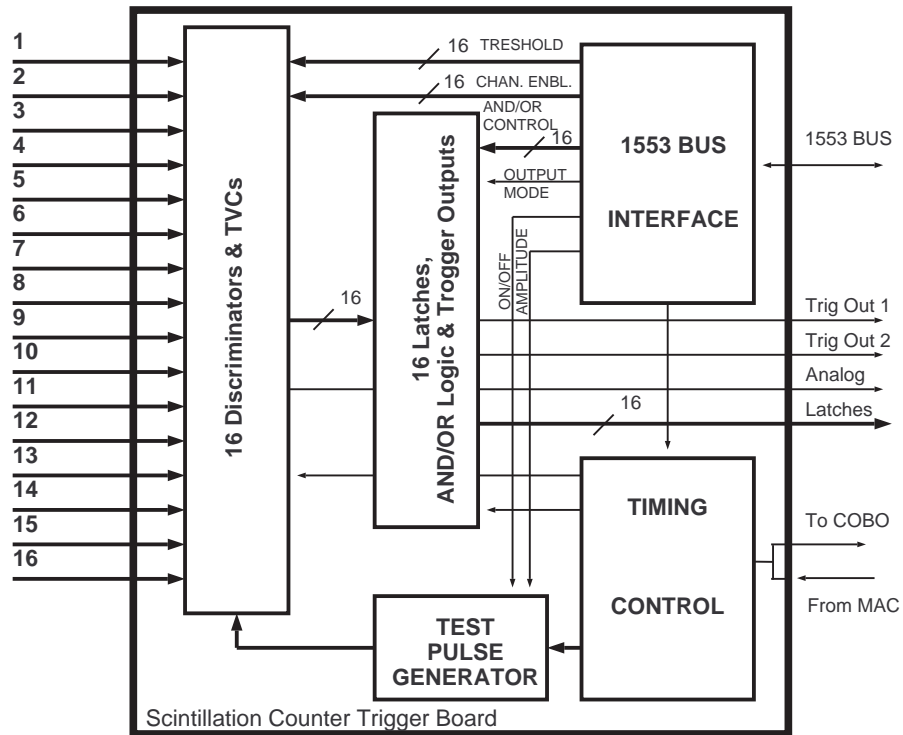


Fig. 10. The block diagram for the scintillation counter trigger board.

Each SCTB channel had an amplifier/discriminator, trigger latch and time-to-

voltage converter (TVC) (see Fig. 11). DC isolation of the SCTB inputs from the common HV ground connected to each phototube base was provided. Each input was transformer coupled and has optional jumpers to isolate primary windings from the SCTB ground plane. The threshold level for each channel could be independently and remotely set from 10 mV to 255 mV. Each channel was supplied with a common test signal from the test pulse generator. The amplitude of the signal was digitally controlled which allowed for remote testing of the particular channel during the run.

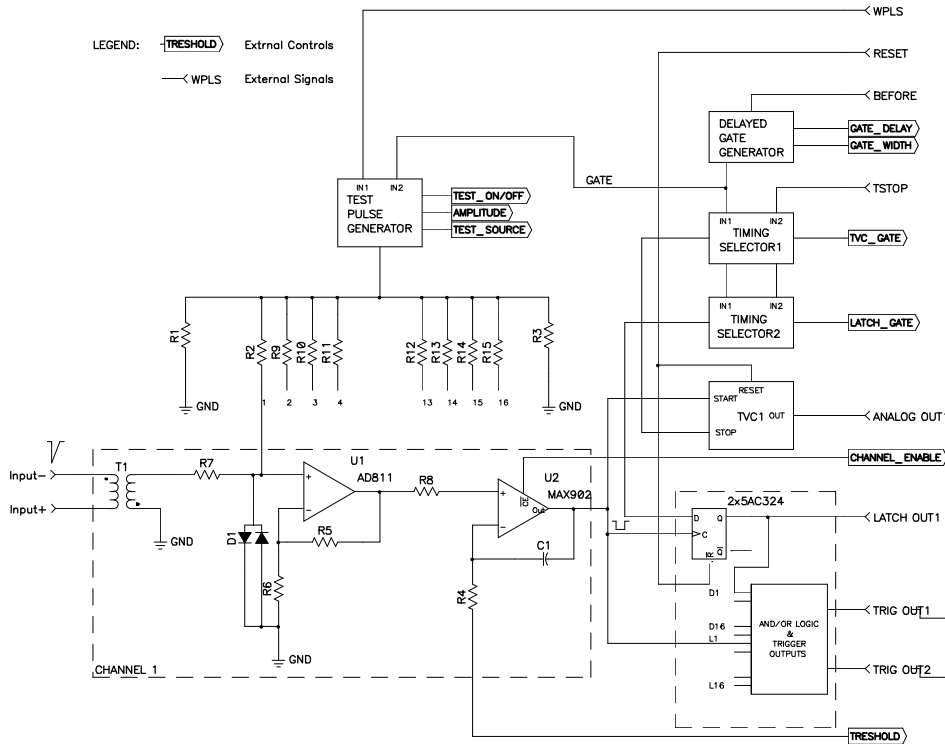


Fig. 11. The diagram of the amplifier/discriminator, trigger latch and TVC for a SCTB channel.

Each SCTB channel had a TVC connected to its discriminator output. There were two TVC ranges available, a 500 nsec range for normal data taking and

a 2  $\mu$ sec range for test purposes. The internal gate width and delay for the 16 channels could be remotely varied up to 510 nsec in 2 nsec steps.

Each of the two trigger outputs produced a 24 mA output signal which exceeds the standard 16 mA NIM requirement. Each pair of the 16 channel latch outputs could be ANDed or ORed depending on the selection of the corresponding bit in the AND/OR selection byte. Eight product signals were then ORed together producing the trigger signal output. Each trigger output had its own AND/OR control byte which can be set separately. The trigger signals from each scintillator board were brought to the NIM logic system described in section 5.4.

The scintillator data, consisting of digitized TVC output and latch bits(see Fig. 10) were recorded using the muon electronics system [1]. This system treated the scintillator counter information as an additional layer of muon PDT for the purpose of data recording.

## 4 Production

### 4.1 Scintillator Testing

One scintillator from each batch was tested prior to having the grooves machined into the surface. The test was performed by placing the scintillator in a light tight box with a 24"  $\times$  24" anodized aluminum sheet placed underneath the scintillator [11]. Using a telescope of three scintillator paddles, a cosmic ray trigger was generated and the light from the scintillator was measured using a 12"  $\times$  12" sheet of Bicron 91A fiber glued together to form a flat surface using optical epoxy [7] and coupled to an EMI 9902KA phototube. The signal area was digitized using a LeCroy QVT and was compared to the signal from a reference sheet of scintillator. The batches tested varied in measured pulse height by less than 6% and no scintillator was rejected by these tests.

### 4.2 Fiber Testing

Every 500 m reel of fiber used in the scintillation counter production was tested. The fiber used in the counters were required to pass a light attenuation and an absolute light output test. In all, 700 samples of fibers were tested

From the test of each 3 m fiber the following quantities were recorded

$$I_3 = \text{Intensity of light for a source at 30 cm} \quad (2)$$

$$I_{15} = \text{Intensity of light for a source at 150 cm} \quad (3)$$

$$I_{27} = \text{Intensity of light for a source at 270 cm} \quad (4)$$

where the equipment used to test the fiber is the same as discussed in section 2.1. Similarly, the three intensities were recorded for special fibers chosen to be used as a reference:  $R_3$ ,  $R_{15}$ , and  $R_{27}$ . The reference fibers were needed to normalize the day to day variations in the fiber testing apparatus. For normalization purposes the following ratios were calculated for each group of fiber measurements

$$IR_3 = I_3/R_3 \quad (5)$$

$$IR_{15} = I_{15}/R_{15} \quad (6)$$

$$IR_{27} = I_{27}/R_{27}. \quad (7)$$

The intensity variation due to the source and photodiode was tracked over a period of 5 months. The relative variation as a function of distance changed during the 5 month testing period but the variation in equations 5, 6, and 7 was minimal.

Deciding whether a particular fiber was accepted depended upon the attenuation length of the fiber and the absolute light output. The attenuation length was measured by calculating the ratio  $I_{15}/I_{27}$  for each fiber. By making a cut of  $I_{15}/I_{27} < 1.6$ , fibers with short attenuation lengths were removed. The results of this cut are shown in Fig. 12. The absolute light output was checked

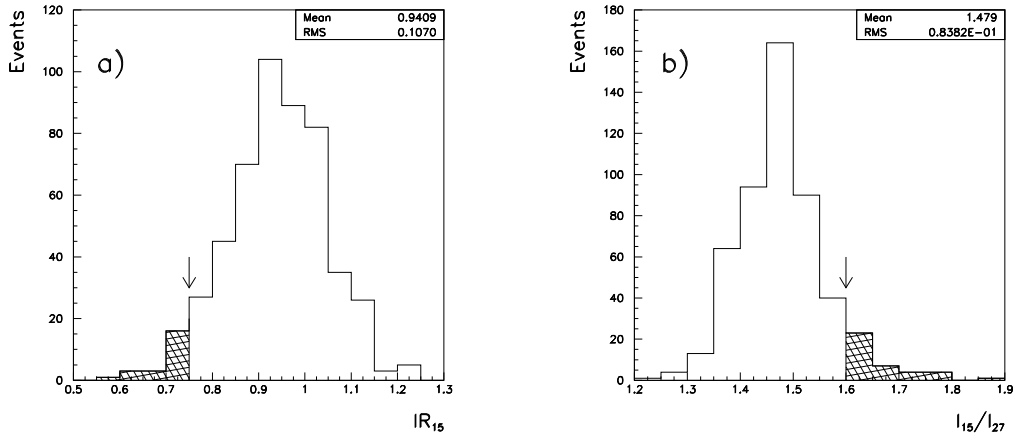


Fig. 12. (a)The distribution of the absolute light output parameter  $IR_{15}$ . (b)The distribution of the attenuation length parameter  $I_{15}/I_{27}$ . The hatched regions are the fibers that were removed by the cuts.

by cutting on  $IR_{15}$  for each fiber. Fibers which had a value below 0.75 were

rejected. The results for this cut are shown in Fig. 12. These cuts rejected about 9% of the fiber tested.

### *4.3 Phototube Testing*

The preliminary testing of the photomultiplier tubes and bases was done at MSU. The aim of this procedure was to check the tubes and bases for proper operation, determine a rough level of dark current noise, determine the voltage at which each tube-base combination provided a  $10^7$  gain, and match the tubes into groups of similar operating voltage.

Tests of proper current, voltage division, and ground connections were made on each base as a final production step by the assembly vendor. In addition, the tube-base output pulses were checked by oscilloscope as part of the test process to verify correct pulse shape characteristics. A practical measure of tube noise was made by powering each tube at its operating voltage in a dark box, applying a threshold of 30 mV to the tube output, and measuring the counting rate. The 30 mV threshold was close to the threshold used on the detector readout electronics.

To determine the operating voltage of the tubes, a LED test assembly was constructed. A green (562 nm) LED was installed in an aluminum endpiece, which was inserted in the end of the mu-metal shield and fixed in place. The LED was recessed and centered within the endpiece so that a phototube inserted into the shield and butted up against the endpiece was a constant distance from the light source. This assembly was then mounted inside the dark box. A fast (8 nsec) voltage pulse with a 50  $\mu$ sec period was applied to the LED to provide an input light pulse. The charge of the output tube pulses was read out using a QVT multi-channel analyzer with an internal threshold of 30 mV. A Hamamatsu R580-17 tube, previously measured for gain and output charge, was used as a reference to calibrate the system. The operating voltage of the EMI tube was defined as the voltage at which that tube gave an output pulse equal to that of the Hamamatsu PMT. Additionally, pulse height measurements were made at +50 V and -50 V around the operating voltage to provide information on the gain variation. Of the 800 tubes delivered 10 did not have any response and about 50 had operating voltages above the maximum allowed value of 1600 V. These tubes were replaced by the vendor.

### *4.4 Production Testing*

A light leak test of the counters was done after a counter was completed. The test used a bank of fluorescent lights and scalars to check for leaks. The

counters were then placed in a light tight box which allowed for the simultaneous test of three counters. A Digital VAXstation Model 3100 was used to control the testing electronics and to store the test results. The workstation interfaced with the CAMAC equipment through a Jorway Model 111 PDP-11/CAMAC interface. Since the objective of the production test was to verify the counter performance, six reference phototubes and bases, with an absolute gain within a 10% range were used. The counter testing was performed using cosmic ray telescopes consisting of three counters in coincidence (two above and one below the testing box) at five locations (the middle of the counter and each of the four corners). A trigger was formed by the logical OR of the five telescopes, and events with more than one telescope hit were rejected offline. A pattern unit was used to record which counters and telescopes were hit. The information from the pattern unit was then used to determine the efficiency of the counters (number of counter hits divided by number of triggers) as a function of position. CAMAC ADC's and TDC's were used to measure the pulse height and timing for each tube. When combined with the pattern unit information, these values could be determined at each telescope position. CAMAC scalers were also used to monitor all the rates. A completely automated procedure was developed to run the test. Two runs, each lasting three hours, were performed on each set of counters with the high voltage set at the nominal value and nominal minus 200 V. These two points allowed a relative comparison to be made between all counters. The counters were all found to have efficiencies near 100% and the overall variation of the counters was small. The only counter rejected by the tests was one that was deliberately built with sub-standard fibers, and consequently showed a reduced pulse height.

Figure 13 shows a typical integrated pulse height distribution for the 81" and 113" counters for cosmic rays passing through a corner and through the center of the counter. The distribution of the minimum peak pulse height from any location on the counter is shown in Fig. 14. The counter to counter variation in minimum pulse height is due mainly to differences in the fiber and phototube cathode. The amount of charged collected even at the poorest location on the counter is sufficient to maintain a high efficiency. A measurement of the photoelectron yield, on a prototype counter, gave 29 to 31 photoelectrons at the center of the counter decreasing to 18 to 22 photoelectrons at the corners of the counter (see Fig. 15).

#### 4.5 *Final Testing*

A final test before installation was performed on each completed counter using the same testing equipment described in section 4.4, except that the standard phototubes were replaced with the final phototubes for that counter. The counter was tested at the nominal voltage for each tube and then nominal

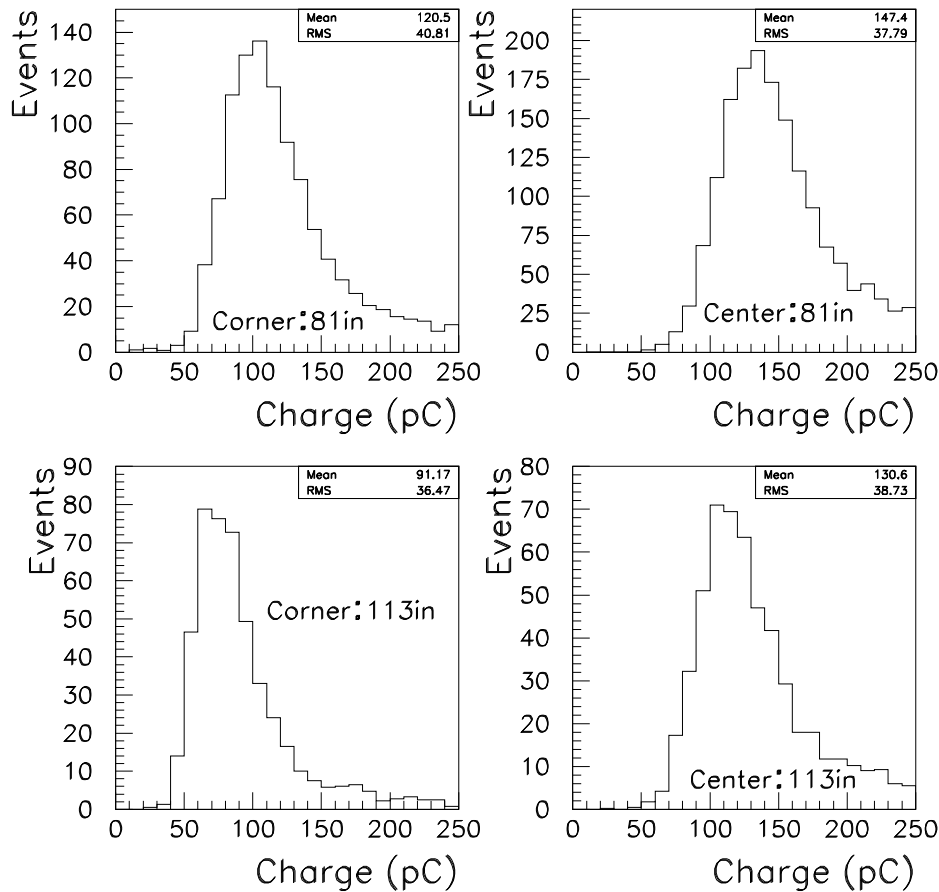


Fig. 13. The pulse height distributions for the corner and center of the 81" (top) and 113" (bottom) counters.

minus 100, 200, and 300 V. This test verified that the nominal voltage was  $\sim 100\%$  efficient and gave the turn on curve for the counter. This turn on curve allows thresholds adjustments to be made online without compromising efficiency. The photomultiplier HV were adjusted so that each tube operated approximately 150 V above the knee of the plateau curve.

## 5 Commissioning Tests and Initial Results

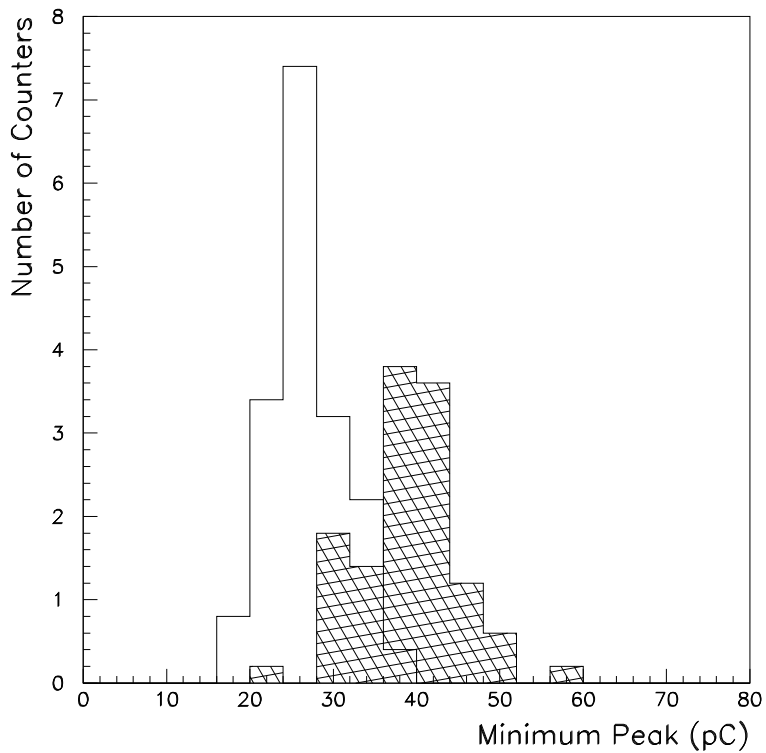


Fig. 14. The minimum pulse height distribution for the 81" (hatched) and 113" counters.

19/20		18/19
19/18	31/29	20/18
18/22		18/18

Fig. 15. The photoelectron yield at different locations along the counter. The two numbers are the yield given by each photomultiplier tube on the counter.

### 5.1 Phased Installation

The muon scintillation counters cover 6 of the 8 octants in the central muon detector. Octants 0, 1, and 2 were installed at the beginning of the Run 1b and octants 3, 4, and 7 were installed during the run. Octant 3 was operational by

late February 1994 and octants 4 and 7 were operational by December 1994 and March 1995 respectively. Each octant consists of 40 scintillation counters mounted on 5 PDT modules. The scintillators mounted on the top were 113" long, the scintillators on the upper sides were 108" long, and the scintillators on the lower sides were 81.5" long.

## *5.2 PDT Array Testing*

The initial tests of the counters after installation on the detector involved powering the arrays and measuring the singles (individual PMT) and doubles rates (coincidence between two PMT's) from each counter. This verified each counter was in nominal working condition and was not damaged during installation. Plots of counter hits and hit timing during data taking verified that the counter system was working. The time difference between the two phototubes on the same counter was a useful measure of counter performance, with an abnormally large width indicating a problem with the counter or TVC.

## *5.3 Tests with 500 nsec and 100 nsec Gate Widths*

In order to time in the counters, data from multiple runs were accumulated and cuts applied to insure that only good reconstructed tracks in the muon system were kept. Initially the gate width for the electronics was set at 500 nsec to insure that the in time particles would be within the gate. The initial plots of the timing for the counters showed that in addition to the in-time muon peaks there were beam halo and backscatter peaks. These will be discussed later in section 5.6.3. After determining the in-time muon peak for the counters, the gate width was reduced in steps to 200 nsec and finally to 100 nsec. The 100 nsec width was used as the final gate width for most of the counters and was not reduced further so that a search for slow moving particles could be made. However, the gate was reduced to 50 nsec for a ring of counters on either end of the detector because those counters had a higher rate of backscatter tracks passing through them.

## *5.4 Results from Scintillator Veto Bit*

Both phototubes on a scintillation counter were required to fire in order for a trigger to be generated for that counter in the scintillator trigger board. The trigger signals from all 8 scintillation counters on a PDT were ORed and the output was sent to two NIM crates in the collision hall. The triggers corresponding to the scintillator counters of a given octant were ORed to produce

a single trigger signal for each of the 6 octants which have counters. These signals were stretched and sent to the Moving Counting House (MCH) outside of the collision hall. In the MCH the signals were fed into logic units in NIM crates. In addition, coarse centroid trigger (CCT) pulses from the muon PDT's were also fed into the logic units. A coincidence of the scintillator trigger pulse for an octant with the corresponding CCT pulse defines a SCINT\_CONFIRM trigger term. An absence of hits in the scintillator octant and the presence of a CCT pulse for that octant defines the SCINT\_VETO trigger term. The final trigger term used for the muon data was a trigger term SCINT\_VETO\_CONFIRM\_BAR which was formed by the presence of the SCINT\_VETO and the absence of the SCINT\_CONFIRM. If there was a valid scintillator-CCT coincidence in any octant, then a veto in any other octant was ignored.

Since the CCT signal was only valid for a short time interval, a gate was used in defining the SCINT\_CONFIRM and SCINT\_VETO terms to insure that no spurious CCT signals would generate false terms. The logic diagram for the veto is shown in Fig. 16.

In addition to the logical veto terms, the scintillator trigger signals and CCT signals for each octant were recorded in one of the data words for use in monitoring the Veto.

### *5.5 Monitoring Scintillation Counters*

The performance of the scintillation counters and the phototube gains were monitored daily. During the daily 30 minute "quiet time", where there was no beam in the accelerator, the AND rates for each of the scintillation counters were recorded by a software program which used the trigger board 1553 bus to selectively disable and enable counters and also place them in the transparent mode where the discriminator signals are ungated. The AND rate for fully efficient counters was dominated by the background radiative photons from the collision hall walls and ceiling. By maintaining the rates at the appropriate level we could insure that the counters were fully efficient. Periodically we lowered the thresholds for counters which were beginning to record a low AND rate to maintain full efficiency. The efficiency verses voltage for a prototype counter placed in the collision hall is shown in Fig. 17 and also shown is the AND rate for the same counter.

As the photomultiplier tubes aged we observed that the gain of some of the tubes was dropping quite rapidly. To study this, two sample tubes were tested as a function of the anode current by using the equipment described in section 4.3. The gain verses integrated anode current for a EMI 9902KA tube,

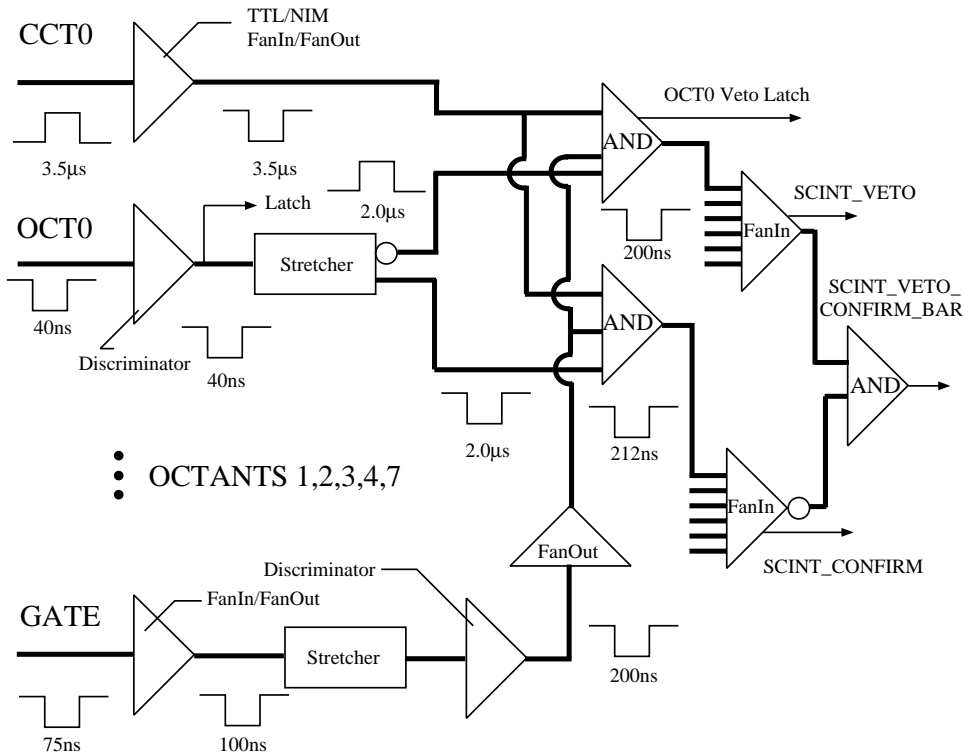


Fig. 16. The diagram detailing the logic used in the trigger.

which have CsSb dynodes, is shown in Fig. 18. For this test the EMI 9902KA was run at two voltage values. Also shown is the response for a EMI 9903KA tube which has BeCu dynodes. Other than the rapid initial loss in gain as a function of integrated anode current, the EMI 9902KA tubes have operated without problems. Of the 480 tubes in the system only 3 tubes have failed during the run.

In addition to AND rates the voltages and currents of the HV supplies which powered the counters were monitored at the same time. The ratio of voltage divided by the current was monitored to check for constancy over time. This ratio was used to find HV channels which drifted due to moisture being absorbed into the voltage feedback resistor of the HV supply. This monitor was sensitive to drifts of 10 V or greater.

### 5.6 Counter Performance

The offline analysis is broken into two parts. The first is the calibration of the timing for the counters and determination of the efficiency of each counter. The second deals with using the scintillator as a tool to improve the purity of

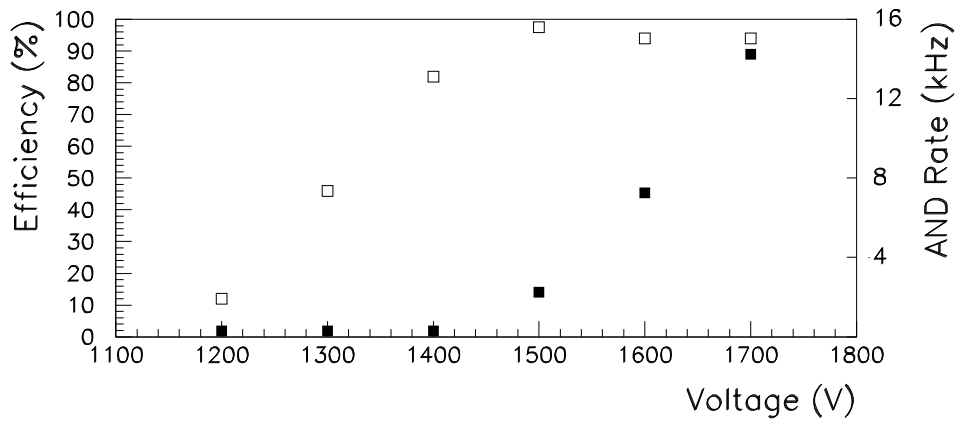


Fig. 17. The efficiency (open squares) and AND rates (closed squares) for a prototype counter as a function of the applied High Voltage.

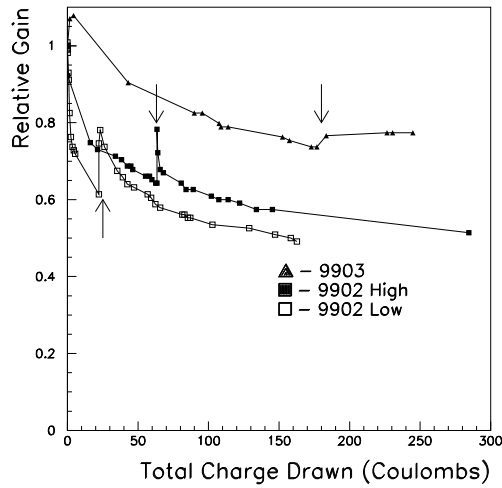


Fig. 18. The relative gain as a function of the total charge drawn for a EMI 9903KA and 9902KA phototubes. The 9902 phototube was run at two voltage values. The arrows indicate a two week span when the phototube was powered off.

the muon sample.

### 5.6.1 Timing Calibration

The time-to-voltage converters of the muon scintillator electronics were stopped by a Tevatron clock pulse synchronized to the average beam crossing time. The voltage was then converted to a digital signal by an analog to digital converter(ADC). The time recorded by the electronics includes the time-of-flight of the muon from the interaction point to the scintillator( $T_{TOF}$ ), the propagation time of the light in the fiber( $T_{fiber}$ ), and the time delay in the cable and electronics. A scintillator time  $T_{\mu-scint}$ , which corresponds to the time-of-flight of the muon, was calculated from the ADC counts by using the conversion

$$T_{\mu-scint} = T_{slope} \cdot (T_0 - T_{ADC}) - T_{fiber}. \quad (8)$$

where  $T_{ADC}$  is the scintillator time in ADC counts, and  $T_{slope}$  is a constant, used to convert the ADC counts to time in nanoseconds. The  $T_0$  was a counter by counter time offset chosen so that the average  $T_{\mu-scint}$  corresponded to the average time of flight from the interaction point to the scintillation counter. An initial  $T_0$  value was extracted from the intercept of the calibration fit with the cable delay time. Collider muons were then used to refine the  $T_0$ 's by taking the difference between the expected time and the observed.

Muons detected in the collider data were used to measure systematic variations in the timing across the face of the counter. This was done after the time of flight and a linear fiber light propagation correction had been applied to the data. These variations result in non-zero values for the time difference  $\Delta T_{\mu-scint}$  between  $T_{\mu-scint}$  and the time-of-flight defined as

$$\Delta T_{\mu-scint} = T_{TOF} - T_{\mu-scint}. \quad (9)$$

An asymmetry in the timing occurs due to the different fiber lengths used to readout the two halves of the scintillator. The fiber from one end must make a U-turn to reach the phototube and the fiber from the opposite end does not. Shown in Fig. 19 is  $\langle \Delta T_{\mu-scint} \rangle$  versus the position along the length of the scintillator. The origin is taken to be the center of the counter. The discontinuity is consistent with the fiber from one end of the counter being about 10" longer than from the other end. Figure 19 also shows  $\langle \Delta T_{\mu-scint} \rangle$  versus the position along the breadth of the counter where zero is the center of the counter. The breadth variation is due to longer fiber lengths to phototube for fibers further from the center of the counter. Each of these figures was fit with a second order polynomial and used as a correction to the time.

The results of these calibrations are shown in Fig. 20. The top plot shows the raw time distribution from the scintillator and the bottom plot is the corrected

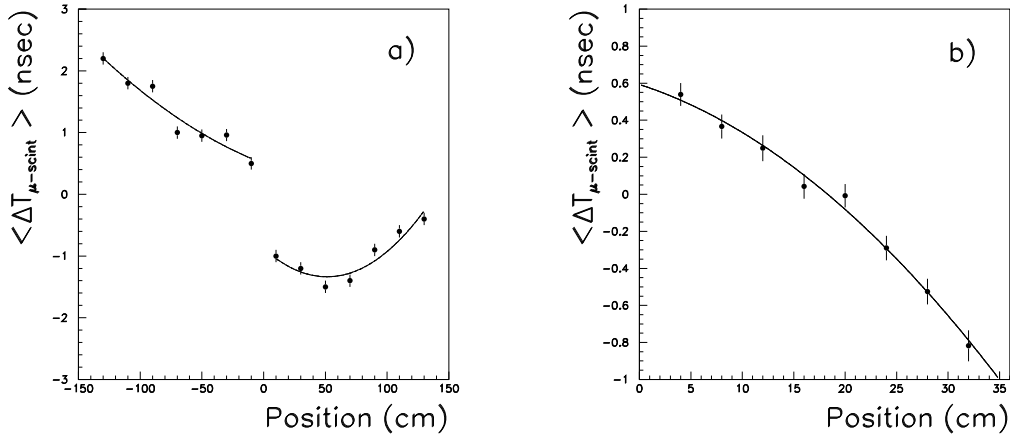


Fig. 19. The mean  $\Delta T_{\mu-scint}$  versus (a) the position of the muon hit along the length of the counter and (b) along the width of the counter. The zero position corresponds to the center of the counter.

timing distribution. The result of the calibration procedure is an improvement in the resolution by approximately a factor of two. This allowed the timing cuts on the scintillator to be narrowed thereby eliminating additional background events.

### 5.6.2 Counter Efficiency

The efficiency of the counters has been measured using collider muons. The muons used in the study are required to pass standard  $D\bar{O}$  quality cuts and point to an octant instrumented with scintillation counters. Track quality requirements are necessary to ensure a good sample of muon tracks. Poorly reconstructed tracks can fake muon scintillator inefficiency by reconstructing away from the fired counter. The efficiency is calculated for each counter as the fraction of reconstructed tracks pointing to the counter that have a valid hit from either photomultiplier tube. The global muon scintillator efficiency from summing over tracks hitting all counters is  $98.4 \pm 0.2(stat.)\%$ . We also note that for 98.1% of the tracks both phototubes fired.

There are a number of reasons why the scintillator counters may be incorrectly registered as inefficient:

- (1) Cosmic ray muons or other out-of-time tracks could fall within the 900 nsec gate of the PDT but not the 100 nsec gate of the scintillator.
- (2) Cracks between scintillator counters on a chamber.
- (3) Spurious tracks from reconstruction or other sources.
- (4) The intercept location of the muon track on the scintillator counters is

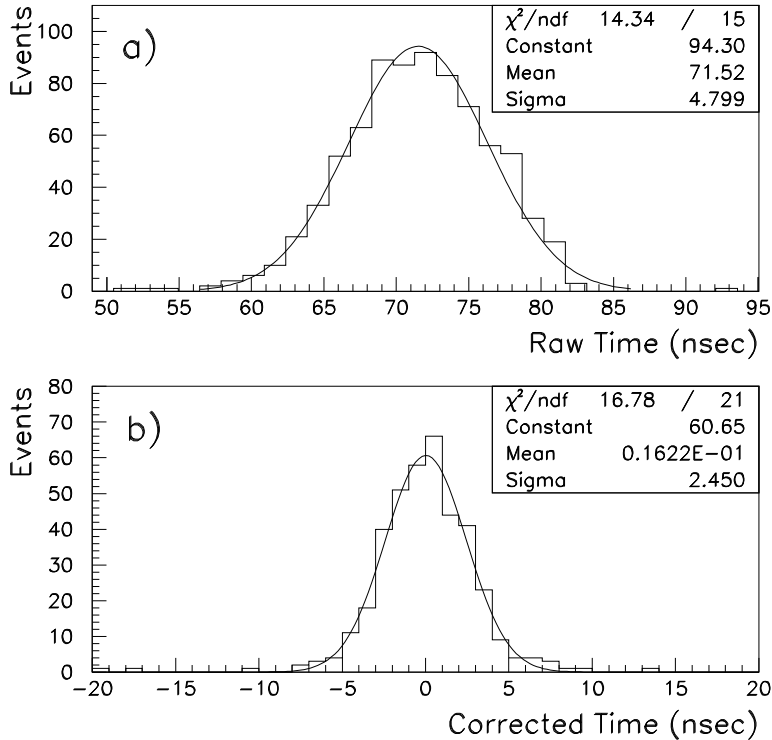


Fig. 20. (a) The raw time distribution for an 81" counter. And (b) shows the corrected time.

reconstructed incorrectly and the fired scintillator is not matched to the track.

Given these effects we estimate the true counter efficiency as greater than 99%. The counter efficiency was also determined to be independent of the track position in the counter.

### 5.6.3 Background Rejection

The scintillation counters do an excellent job of rejecting backgrounds to the muon sample. The backgrounds are from cosmic rays and accelerator related effects such as beam halo and backscattered particles. The beam halo tracks traverse the detector along with the protons involved in the collision and arrive early relative to the events associated with the interaction. The backscatter particles were produced by particles from the interaction, striking the inner radius of the calorimeter, beam collimators and the accelerator quadrupole magnets at either end of the detector. Because of the extra distance, the backscatter particles arrive later than the events coming directly from the

interaction.

The fast timing information of the scintillator allow the time-of-flight of the muon to be used as a discriminator against all three of the mentioned backgrounds. Figure 21 shows the difference in the time-of-flight of flight for a sample dimuon events. The fit is to a Gaussian plus a zeroth order polynomial. The percentage of cosmic muons within a two standard deviation cut is only 1.4%.

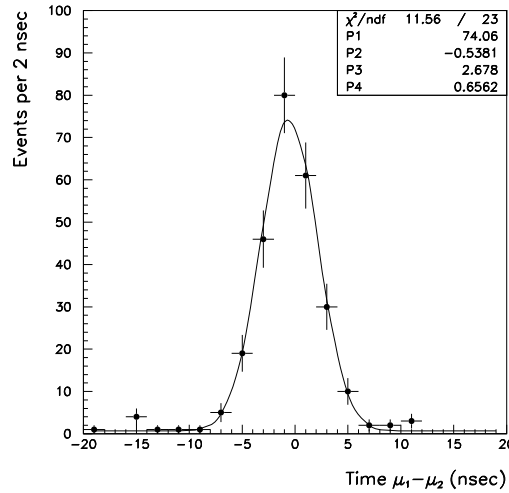


Fig. 21. The difference in scintillator times for a sample of dimuon events.

Figure 22 shows the raw time distribution of hits on a scintillator counter near one end of the detector and a counter near the center of the detector. The three distinct peaks are due to beam halo, backscatter, and in-time events. The ring of counters near each end of the detector had the most backscatter tracks passing through them. Counters near the center of the detector did not have such large backscatter peaks as they were shielded from the backscatter sources by the calorimeter and iron toroid. The beam halo peak was reduced substantially after these plots were made by tuning of the accelerator and by installing new shielding walls just outside the detector in the accelerator tunnel. For Run 2, new shielding will be installed inside the detector which is expected to reduce the backscatter by approximately a factor of 50.

The effect of the scintillator veto on the first level muon trigger was substantial. The high  $p_T$  dimuon trigger was reduced by approximately a factor of 3 when the veto for the top four octants were added to the trigger. The low  $p_T$  dimuon trigger was reduced by a factor of approximately 1.6.

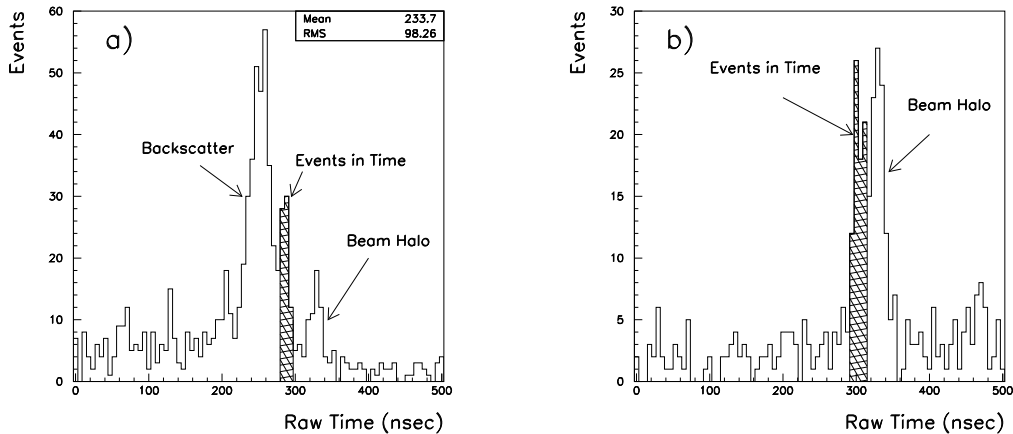


Fig. 22. (a) The raw time distribution of hits where the three peaks are due to beam halo, backscatter, and in-time events for a counters near one end of the detector. (b) And the raw time distribution for a counters that are near the center of the detector.

## 6 Summary

The scintillation counters built for the DØ Muon System worked very well during the latest data taking run. The scintillator and fiber design chosen performed as expected. The phototubes chosen had a rather sharp gain variation during the initial running but were stable after the initial burn-in period. The scintillators were effective in rejecting background from cosmic rays, out-of-time accelerator muons, and backscatter particles, while maintaining an efficiency greater than 99%.

## Acknowledgements

We thank the staffs at Fermilab and the collaborating institutions for their contributions to this work, and acknowledge support from the Department of Energy and National Science Foundation (U.S.A.), CNPq (Brazil), Departments of Atomic Energy and Science and Education (India), and CONACyT (Mexico). We also thank A. Galyaev who worked with us on the photocathode measurements.

## References

- [1] S. Abachi *et al.* (DØ Collaboration), Nucl. Instr. and Meth. A 338 (1994) 185; C. Brown *et al.*, Nucl. Instr. and Meth. A 279 (1989) 331; J.M. Butler *et al.*, Nucl. Instr. and Meth. A 290 (1990) 122.
- [2] Type 404A plastic scintillator, Bicron Corporation, 12345 Kinsman Rd, Newbury, OH 44065-9677.
- [3] Adapt Plastics, Rockford, IL.
- [4] Central Workshop, Bhabha Atomic Research Center, Bombay, India.
- [5] Type BCF91A waveshifter fiber, Bicron Corporation, 12345 Kinsman Rd, Newbury, OH 44065-9677.
- [6] Type Y-11 double clad waveshifter fiber, Kuraray of America, Inc., Subsidiary of Kuraray Co., LTD., Osaka, Japan, 200 Park Ave., New York, NY 10166.
- [7] BC-600 Optical Epoxy, Bicron Corporation, 12345 Kinsman Rd, Newbury, OH 44065-9677.
- [8] 5-Minute Epoxy, ITW Devcon, 30 Endicott St., Danvers, MA 01923.
- [9] Department of Physics and Astronomy, Michigan State University, East Lansing, MI 48824.
- [10] Hitech Elmech Pvt. Ltd., 67A Ranade Rd, Bombay, 400 028 India.
- [11] Everbrite anodized aluminum, Alcoa Brite Products Inc., 3040 Northwoods Parkway, Norcross, GA 30071.
- [12] Tyvek 1055B, E.I. Dupont De Nemours & Co., 705 Canter Rd., Rt 141, Wilmington, DE 19810-1025.
- [13] We thank J. Freeman for suggesting the use of Tyvek to us. We thank Herman White for providing us with his test results of the reflectivity of the various types of Tyvek produced by Dupont.
- [14] B-Line Systems, Inc., Highland, IL 62249
- [15] Al Bross, private communication.
- [16] Model 6035 Hg(Ar) pencil source, Oriel Corp., 252 Long Beach Blvd., P.O.Box 872, Stratford, CT 06497-0872.
- [17] Model 221 silicon photodiode, Antel Optronics Inc., 3310 South Service Rd., Burlington, ON, Canada.
- [18] BC-630 Silicone Optical Grease, Bicron Corporation, 12345 Kinsman Rd, Newbury, OH 44065-9677.
- [19] Thorne EMI Glencom Inc., 23 Madison Rd., Fairfield, NJ 07866
- [20] Hamamatsu Corp., 360 Foothill Rd., PO Box 6910, Bridgewater, NJ 08807
- [21] CFC Inc., Waltham, MA. 02254.
- [22] Mitech Electronics Corporation, 411 Washington St., Otsego, MI 49078.
- [23] Magnetic Shield Corp., 740 North Thomas Dr., Bensenville, IL 60106.